Ibañez *et al.*
Terrestrial, Atmospheric and Oceanic Sciences (2023) 34:24
https://doi.org/10.1007/s44195-023-00056-0

Terrestrial, Atmospheric and Oceanic Sciences

ORIGINAL ARTICLE

Open Access

Development of quantitative precipitation estimation (QPE) relations for dual-polarization radars based on raindrop size distribution measurements in Metro Manila, Philippines

Marco Polo A. Ibañez[1*], Samuel C. Martirez[1], Alvin G. Pura[1], Ramjun A. Sajulga[1], Esperanza O. Cayanan[1], Ben Jong-Dao Jou[2] and Wei-Yu Chang[3]

Abstract

Quantitative precipitation estimates (QPE) can be further improved using estimation algorithms derived from localized raindrop size distribution (DSD) observations. In this study, DSD measurements from two disdrometer stations within Metro Manila during the Southwest monsoon (SWM) period were used to investigate the microphysical properties of rainfall and develop localized dual-polarimetric relations for different radar bands and rainfall types. Observations show that the DSD in Metro Manila is more distributed to larger diameters compared to Southern Luzon and neighboring countries and regions in the Western Pacific. This is reflected by the relatively higher mass-weighted mean diameter (D_m) and smaller shape (μ) and slope (Λ) parameters measured in the region. The average values of D_m and normalized intercept parameter (N_w) in convective rain samples also suggest that convective rains in Metro Manila are highly influenced by both continental and oceanic convective processes. Dual-polarimetric variables simulated using the T-matrix scattering method showed good agreement with disdrometer-derived reflectivity (Z_H) values. The 0.5 dB and 0.3° km^{-1} thresholds for the differential reflectivity (Z_{DR}) and specific differential phase (K_{DP}) based on the blended algorithm of Cifelli (J Atmos Ocean Technol 28:352-364, 2011) and Thompson et al. (2017) are proven to be useful since the utility of the dual-polarimetric variables as rainfall estimators are shown to have dependencies on the radar band and rainfall type. Evaluation of the QPE products with respect to the C-band shows that R (K_{DP}, Z_{DR}) has the best performance among the dual-pol relations and statistically outperformed the conventional Marshall & Palmer relation [$R(Z_{MP})$]. The results show that dual-polarimetric variables such as Z_{DR} and K_{DP} can better represent the DSD properties compared to one-dimensional Z, hence providing more accurate QPE products than the conventional $R(Z)$ relations.

Keywords Raindrop size distribution, Dual-polarization relations, Quantitative precipitation estimates, PARSIVEL^2 disdrometer

*Correspondence:
Marco Polo A. Ibañez
marcopoloibanez@gmail.com
Full list of author information is available at the end of the article

1 Introduction

The geographical location of the Philippines makes it susceptible to rainfall-inducing weather systems such as Tropical cyclones and Monsoons (Bagtasa 2019; Cayanan et al. 2011). Heavy rainfall is frequently experienced in Metro Manila during the Southwest Monsoon (SWM) period (Cruz et al. 2013). The SWM, locally known as *Habagat*, brings significant amounts of rainfall during the months of June to September in the western regions of the Philippines (Matsumoto et al. 2020). Asuncion and Jose (1980) reported that 43% of the average annual rainfall in the Philippines is derived from the SWM period. While rainfall is a valuable water resource, it remains a disaster threat during extreme rainfall events (Jamandre and Narisma 2013). It is essential, therefore, to have accurate rainfall estimates in the country, especially in the highly-urbanized area of Metro Manila. Measurements from rain gauges are usually considered to be the reference rainfall (Villarini et al. 2008). However, due to gaps in observation sites and time resolution of data, rain gauges are limited in providing accurate rainfall measurements for a wide range of areas. Satellite-derived rainfall measurements are also used to provide rain information at a global scale. However, satellite observations are not always available in real-time and are limited to lower spatial resolutions (Macuroy et al. 2021). High-quality rainfall measurements are important in numerical weather prediction models and hydrometeorological applications (Lee et al. 2019). Hence, it is necessary to have simultaneous rainfall observations with higher temporal and spatial resolution. Polarimetric weather radars are preferred over rain gauges and satellites in producing Quantitative Precipitation Estimates (QPE) because of their ability to cover a larger spatial range and provide real-time rainfall information (You et al. 2022). Weather radars estimate rainfall by measuring the resulting reflectivity (Z) scattered by raindrops within a scanning volume measured in decibels relative to Z (dBZ). One of the most common methods of retrieving rainfall from radar reflectivity is the use of Reflectivity-Rain rate ($R(Z)$) relations. The $R(Z)$ relation is often expressed as a power law ($Z = a^{*}R^{b}$), wherein the values of a and b vary for different seasons, locations, and weather systems. Globally, the most used $R(Z)$ relations are the Marshall & Palmer relation ($Z = 200^{*}R^{1.6}$; Marshall & Palmer 1948), Rosenfeld tropical relation ($Z = 250^{*}R^{1.2}$, Rosenfeld et al. 1993), and the United States WSR-88D radar network relation ($Z = 300^{*}R^{1.4}$, Ulbrich & Lee 1999). However, using a single $R(Z)$ relation may result in inaccurate rainfall estimates since Z is highly variable for different rain types and locations (Seela et al. 2017). Hence, it is highly recommended to calibrate the $R(Z)$ relationship for a specific region in order to improve its performance in rainfall retrieval (Ji et al. 2019).

In addition to the conventional $R(Z)$ relations, rainfall can also be estimated from dual-polarimetric variables (will be referred to as dual-pol variables from hereon). Dual-pol relations are known to have advantages over the conventional $R(Z)$ relation (Zhang et al. 2019). Dual-pol variables such as differential reflectivity (Z_{DR}) and specific differential phase (K_{DP}) can be used to estimate rain rate (R) with greater accuracy because they can constrain environmental factors such as signal attenuation and partial beam blocking as compared to the single-polarization Z (Thompson et al. 2018). The radar parameters being used for rainfall retrieval are related to the microphysical characteristics of rainfall thru the raindrop size distribution (DSD), which is a fundamental property of rainfall defined as the number concentration of raindrops as a function of diameter (Tapiador et al. 2010). DSD variability reflects the relative importance of governing microphysical processes such as collision-coalescence, drop break-up, evaporation, and cloud ice-water interactions (Houze 2014). The DSD also varies with rainfall type (i.e., stratiform and convective), seasons, and topography (Thurai et al. 2016). Bringi et al. (2003) demonstrated that convective rainfall over tropical oceans is characterized by a higher number concentration of smaller raindrops ($D < 1$ mm) compared to continental locations. Moreover, Seela et al. (2018) and Zeng et al. (2019) reported relatively larger raindrops during the summer monsoon compared to the winter monsoon in Northern Taiwan and the South China Sea, respectively. Marzuki et al. (2013) and Seela et al. (2017) also reported terrain-induced convection resulting to drop size enhancements in Indonesia and Taiwan, respectively. More recently, Ibanez et al. (2023) reported larger raindrops in Clark, Pampanga compared to Metro Manila, which also demonstrates the effects of terrain-enhanced convections on the DSD.

In terms of radar applications, DSD measurements are of great importance in having accurate rainfall retrievals since Z is proportional to the sixth moment of the raindrop diameter (Hachani et al. 2017; Wu et al. 2018). Disdrometers are commonly paired with weather radars as they can explicitly measure the fall velocities and diameter of precipitation. (Tokay et al. 2013; Thompson et al. 2015). Integral rainfall parameters (IRPs) such as rain rate (R, mm h^{-1}), total number concentration (N_t, m^{-3}), liquid water content (LWC, g m^{-3}), and reflectivity factor (Z, mm^{-6} m^{-3}) can also be derived from disdrometer measurements (Angulo-Martinez et al. 2018). You et al. (2018) derived dual-pol parameters and relations for different rainfall events in a coastal area in Korea using an optical disdrometer. It was found that using a linear ensemble method composed of $R(Z, Z_{DR})$ and $R(K_{DP})$ provided

more accurate QPE than the conventional $R(Z)$ relation. The applicability of Z_{DR} and K_{DP} for tropical oceanic rain also was studied by Cifelli et al. (2011) (hereinafter C11) by creating a blended QPE algorithm based on continental convection in Colorado. Thompson et al. (2015, 2018) (hereinafter TH15 and TH18, respectively) hypothesized that smaller raindrops observed in the Tropical oceans resulted in lower values of Z_{DR} and K_{DP} for a given *LWC*. Hence, TH18 lowered the threshold values of C11 for Z_{DR} in order to utilize it and explore precipitation in the Tropical Ocean. Previous radar QPE studies in the Philippines used pre-calculated values derived from other areas (Heistermann et al. 2013; Crisologo et al. 2014). The recent study of Macuroy et al. (2021) (will be referred to as MC21 from hereon) was the first study in the country to derive dual-pol parameters from DSD measurements using an optical disdrometer during the wet period in Southern Luzon. Results showed that although the $R(Z)$ relation performed well in terms of correlation and root mean square error, the $R(K_{DP})$ relation statistically outperformed other relations and provided more accurate QPE. However, the results of the study are only limited to a single radar wavelength (i.e., C-band) and do not necessarily reflect the optimal QPE relations and DSD properties for other regions in the Philippines. Notably, the DSD properties and their application in calibrating dual-pol rainfall relations are rarely explored for Metro Manila.

In this study, the DSD characteristics in Metro Manila during the SWM period were investigated using measurements from two optical disdrometers installed in Science Garden and La Mesa watershed, Quezon City. The impacts of DSD variability on dual-pol parameters were also investigated in order to develop dual-pol rainfall estimators for S-, C-, and X-band radars using the T-matrix method (Waterman 1971; Mishchenko et al. 1996). Considering the modernization program of the country's weather bureau (i.e., Philippine Atmospheric, Geophysical, and Astronomical Services Administration or PAGASA), the DSD properties and rainfall estimators for different radar bands presented in this study can serve as a reference in optimizing the disdrometer and dual-pol radar network in different parts of the country. This study is organized as follows. Section 2 provides a brief discussion of the study site and data, which includes data cleaning and processing, and the calculation of IRPs and dual-pol radar parameters. The effects of DSD variability on the resulting radar parameters and rainfall estimators, as well as the utility of the dual-pol relations in different radar bands and rain types, are discussed in Sect. 3. Finally, Sect. 4 summarizes the results and provides the conclusion.

2 Data and methods

2.1 Instrumentation, data set, and study site

The DSD measurements during the wet period in Metro Manila (i.e., June–September) from 2020 to 2022 are collected from the 2nd-generation Particle Size Velocity Disdrometer (hereafter referred to as PARSIVEL^2 disdrometer) installed in Science Garden, Quezon City (14.6° N, 121.04° E, 48 m.a.s.l.) and in La Mesa watershed, Quezon City (14.7° N, 121.07° E, 65 m.a.s.l.) (Fig. 1).

The PARSIVEL^2 is an optical disdrometer that simultaneously measures the size and fall velocities of precipitation with a 1-min sampling interval. However, due to limitations in data transmission, the disdrometers used in this study were programmed to average the 1-min DSD measurements into 5-min samples. The measured raindrop diameter and fall velocities are stored in 32×32 diameter-velocity (D-V) bins with uneven intervals ranging from 0.062 to 24.5 mm and 0.05 to 20.8 m s^{-1}, respectively. The first two bins that correspond to sizes less than 0.25 mm are left empty by the manufacturer because of the low signal-to-noise ratio (Loffler-Mang & Joss 2000). The PARSIVEL^2 disdrometer is preferred over other disdrometer types and its first version model because of its better agreement with rain gauges and improved accuracy in measuring smaller raindrops (Tokay et al. 2014). To reduce sampling errors, the DSD measurements underwent data quality control (QC) procedures following the methods of previous studies (Seela et al. 2017; Angulo-Martinez et al. 2018). The QC procedure includes the removal of the following: (1) raindrops with diameters greater than 8 mm, (2) raindrops that have diameter and fall velocity values outside the 50% spread of the theoretical D-V curve of Beard (1976), and (3) DSD measurements corresponding to rain rates less than 0.1 mm h^{-1} and number concentration less than 10 m^{-3}. 5-min DSD samples within the 1000 km effective radius of tropical cyclones (TCs) were also not included in the analysis as TC-induced rainfall is known to have different microphysical properties (Janapati et al. 2021). It was also reported by Ibanez et al. (2023) that there are no pronounced differences in the DSD properties observed between Science Garden and La Mesa watershed, hence the DSD measurements from the two disdrometer stations were combined. After the QC procedure, a total of 6,850 valid DSD samples were collected from the two stations.

2.2 DSD and integral rainfall parameters (IRPs)

The raindrop concentration per unit volume $N(D_i)$ can be calculated from the PARSIVEL^2 disdrometer using the equation

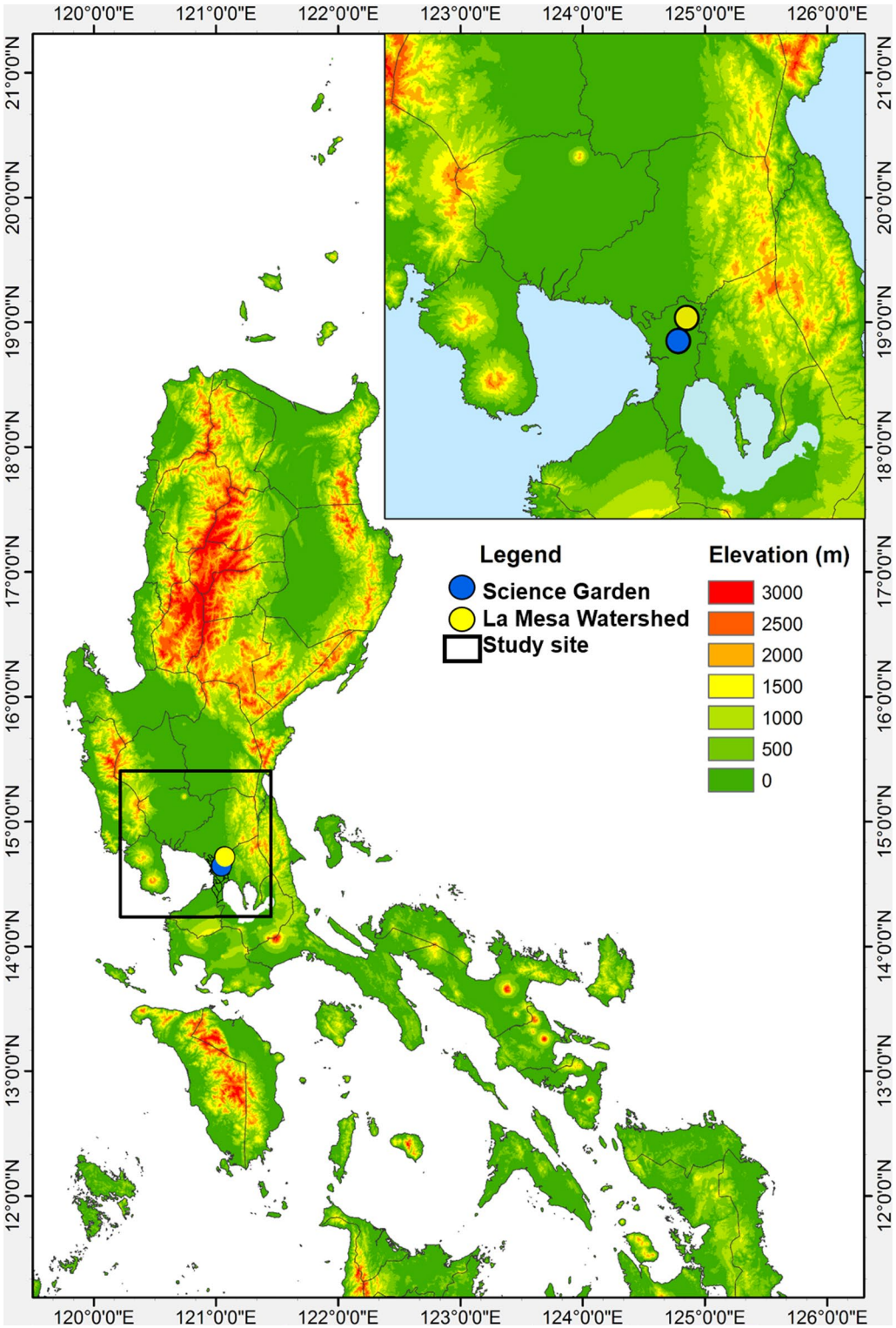

Fig. 1 Digital elevation map showing the locations of the two disdrometer stations within the study site

$$N(D_i) = \sum_{i=1}^{32} \frac{n_i}{v(D_i) A t \Delta D_i} \tag{1}$$

where $v(D_i)$ is the raindrop fall velocity in m s^{-1}, D_i is the raindrop diameter in mm, A is the sampling area ($A = 0.0054$ m^2), t is the sampling time (5 min = 600 s), and ΔD_i is the width of the i^{th} diameter bin. The terminal velocity $v(D_i)$ is approximated using the theoretical D-V curve equation of Beard K.V. (1976) given by:

$$v(D_i) = 9.58\left[1 - exp\left(-\left(\frac{D_i}{0.171}\right)^{1.147}\right)\right] \tag{2}$$

The Integral rainfall parameters derived from the DSD, such as rain rate R (mm hr^{-1}), liquid water content LWC (g m^{-3}), total number concentration N_t (m^{-3}), and reflectivity factor Z (mm^6 mm^{-3}) are calculated from $N(D)$, D_i, and $v(D_i)$ using the following equations:

$$R = 6\pi \times 10^{-4} \sum_{i=1}^{32} v(D_i) N(D_i) D_i^3 \Delta D_i \tag{3}$$

$$LWC = \frac{\pi}{6000} \sum_{i=1}^{32} N(D_i) D_i^3 \Delta D_i \tag{4}$$

$$N_t = \sum_{i=1}^{32} N(D_i) \Delta D_i \tag{5}$$

$$Z = \sum_{i=1}^{32} N(D_i) D_i^6 \Delta D_i \tag{6}$$

The DSDs are parameterized using the widely used Gamma model (Ulbrich 1983) expressed as

$$N(D) = N_0 D^{\mu} \exp(-\Lambda D) \tag{7}$$

where N_0 is the number concentration parameter, μ is the shape parameter, and Λ (mm^{-1}) is the slope parameter. The gamma parameters were calculated using the method of moments expressed as

$$M_n = \int_{D_{min}}^{D_{max}} D^n N(D) dD \tag{8}$$

where n stands for the nth moment of the DSD. A combination of 3.67th, 4th, and 6th moments based on MC21 was used to calculate the gamma parameters using the following equations:

$$\mu = \frac{11G - 8 + \sqrt{G(G+8)}}{2(1-G)}, \tag{9}$$

$$\Lambda = \frac{(\mu + 4) M_{3.67}}{M_4}, \tag{10}$$

$$N_0 = \frac{\Lambda^{\mu+4} M_{3.67}}{\Gamma(\mu + 4)} \tag{11}$$

where:

$$G = \frac{M_4^3}{M_{3.67}^2 M_6^1} \tag{12}$$

The mass-weighted mean diameter D_m (mm) is also computed using the 4th and 3rd DSD moments:

$$D_m = \frac{M_4}{M_3} \tag{13}$$

The normalized intercept parameter N_w (m^{-3} mm^{-1}), which represents the DSD when $N(D)$ approaches the minimum value, is defined by Seela et al. (2017) as

$$N_w = \frac{4^4}{\pi \rho_w} \left(\frac{10^3 LWC}{D_m^4}\right) \tag{14}$$

where ρ_w is the density of water (1×10^3 kg m^{-3}).

2.3 Derivation of dual-polarimetric variables

The dual-pol parameters were derived from the DSD using the openly available PyDSD python package (Hardin 2014). The PyDSD makes use of disdrometer data to retrieve dual-pol parameters (i.e., Z_H, Z_{DR}, and K_{DP}) using the Mueller/T-matrix scattering method (Mishchenko et al. 1996). The process flow of implementing the T-matrix method using the PyDSD package is shown in Fig. 12 in the Appendices. To estimate the dual-polarization parameters using the T-matrix method, conditions such as axis ratio, canting angle distribution, raindrop temperature, diameter range, and corresponding radar frequency and elevation angle must be given. Using the proposed values in MC21, the raindrop temperature was set to be 20 °C, the diameter range was from 0.1 mm to 8 mm, and the elevation angle was set to 0.5°. The average canting angle distribution was assumed to follow a Gaussian distribution with a standard deviation about the mean up to 7.5° (TH15). The raindrop's axis ratio used in this study is assumed to be oblate, which is based on the numerical simulations and wind tunnel tests of Brandes et al. (2002) and can be expressed as a fourth order polynomial equation:

$$\begin{aligned} \gamma =& 0.9951 + 0.0251D - 0.03644D^2 \\ &+ 0.005303D^3 - 0.0002492D^4 \end{aligned} \tag{15}$$

where γ is the axis ratio and D is the raindrop diameter. The dual-pol parameters were calculated for S, C, and X

bands with frequencies 2.80Ghz, 5.61Ghz, and 9.67Ghz respectively.

The Z_H and Z_V, which correspond to the reflectivity factors in the horizontal and vertical polarization in dBZ, were calculated using the equation:

$$z_{H,V} = 10\log\left(\frac{\lambda^4}{\pi^5|K_w|^2}\int_{D_{min}}^{D_{max}}\sigma_{H,V}(D)N(D)dD\right) \quad (16)$$

where λ is the radar wavelength in mm, $\sigma_{H,V}(D)$ is the backscattering cross section for horizontal or vertical polarization and K_w is the dielectric constant of water at 20 °C. The quantities Z_H and Z_V are dependent on the drop diameter D^6 and number concentration $N(D)$ (see Eq. 6). The differential reflectivity (Z_{DR}), which is the logarithmic ratio of Z_H and Z_V expressed in dB (Seliga & Bringi 1976), is expressed as

$$Z_{DR} = 10log\frac{Z_H}{Z_V} \quad (17)$$

The quantity Z_{DR} is zero for spherical drops and increases as the raindrop become more oblate, which usually happens as $D > 1$ mm. The specific differential phase (K_{DP}), expressed in ° km^{-1}, can be calculated using the equation:

$$K_{DP} = \frac{180}{\pi}\lambda\int_{Dmin}^{Dmax} Re\left[\left(f_{vv}(D)\right) - f_{hh}(D)\right]N(D)dD \quad (18)$$

where $f_{hh,vv}$ represents the real parts of the forward scattering amplitude for the horizontally and vertically polarized waves (Vivekanandan et al. 1991). K_{DP} is directly proportional to the LWC and oblateness of the raindrop, and inversely proportional to the radar wavelength; hence K_{DP} is higher at X-band than S-band. The dual-pol relations, $R(Z_H)$, $R(K_{DP})$, $R(Z_H, Z_{DR})$, and $R(K_{DP}, Z_{DR})$ chosen for this study are expressed as

$$R(Z_H) = aZ_H^b, \quad (19)$$

$$R(K_{DP}) = aK_{DP}^b, \quad (20)$$

$$R(Z_H, Z_{DR}) = aZ_H^b Z_{DR}^C, \quad (21)$$

$$R(K_{DP}, Z_{DR}) = aK_{DP}^b Z_{DR}^C, \quad (22)$$

Where *a, b,* and *c* are the coefficient and exponents acquired by applying the least-mean-square fitting method to the polarimetric variables and rain rates calculated from the T-matrix and DSD measurements.

This study also uses the blended optimization algorithm from TH18 and C11 which determines rain estimators used according to the following data quality thresholds.

$R(Z_H)$ if $Z_{DR} < 0.5$ dB and $K_{DP} < 0.3°$ km^{-1}

$R(Z_H, Z_{DR})$ if $Z_{DR} > 0.5$ dB and $K_{DP} < 0.3°$ km^{-1}

$R(K_{DP})$ if $Z_{DR} < 0.5$ dB and $K_{DP} > 0.3°$ km^{-1} and $Z_H > 38$ dBZ.

$R(K_{DP}, Z_{DR})$ if $Z_{DR} > 0.5$ dB and $K_{DP} > 0.3°$ km^{-1}

Although these thresholds are optimized for S-band radars, they are designed to be wavelength independent (TH18). Hence, the algorithms can still be used for C- and X-band radars.

2.4 Statistical evaluation of the derived dual-pol relations

The rainfall values derived from the various relations (R_{est}) in Eqs. (18) to (19) were compared to the rainfall rate retrieved from the DSD measurements (R_{DSD}) (i.e., considered as "ground truth"). In order to evaluate their QPE performance, four statistical validation variables were used in this study, namely: Pearson's correlation coefficient (r), percent bias (pBias), mean error (ME), and root-mean-square error (RMSE).

$$Pearson's(r) = \frac{\sum_{i=1}^{n}\left(R_{DSD} - \overline{R_{DSD}}\right) - \left(R_{est} - \overline{R_{est}}\right)}{\sqrt{\sum_{i=1}^{n}\left(R_{DSD} - \overline{R_{DSD}}\right)^2\sum_{i=1}^{n}\left(R_{est} - \overline{R_{est}}\right)^2}} \quad (23)$$

$$Mean\ error(ME) = \frac{\sum_{i=1}^{n}(R_{est} - R_{DSD})}{n} \quad (24)$$

$$Root\ mean\ square\ error(RMSE) = \sqrt{\frac{\sum_{i=1}^{n}(R_{est} - R_{DSD})^2}{n}} \quad (25)$$

$$Percent\ bias(pBIAS) = \frac{\sum_{i=1}^{n}(R_{est} - R_{DSD})}{\sum_{i=1}^{n}(R_{DSD})} * 100\% \quad (26)$$

r and NSE are dimensionless, ME and $RMSE$ are in mm h^{-1}, and $pBias$ is expressed as a percentage.

3 Results and discussions

3.1 Average DSD characteristics

The average and gamma-fitted DSD during the SWM season in Metro Manila are shown in Fig. 2. The number concentration ($N(D)$) in the y-axis is expressed in a logarithmic scale to account for large variations. The vertical dashed lines represent the raindrop size classification proposed by Krishna et al. (2016). Raindrops with diameters $D < 1$ mm are considered small, $1 \leq D < 3$ mm are midsize, and $D > 3$ mm are large. There is a good agreement between the observed and gamma-fitted DSD. Similar to the values reported by Ibanez et al. (2023),

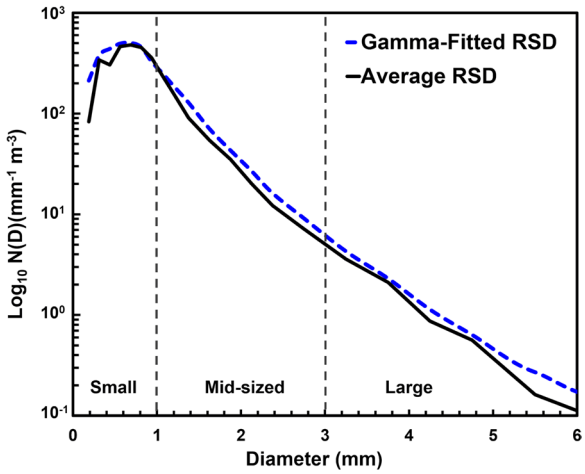

Fig. 2 Average DSD (solid black line) and the fitted DSD using the gamma distribution (blue dashed line) for Metro Manila during the SWM period from 2020 to 2022. The vertical dashed lines represent the raindrop size classification

the average mass-weighted mean diameter (D_m) of the total rainfall in Metro Manila during the SWM period ($D_m = 1.53$ mm) is slightly higher than the value reported in MC21 in Southern Luzon ($D_m = 1.45$ mm) and relatively larger than the values reported by Seela et al. (2017) in Taiwan (1.24 mm) and in Palau (1.11 mm). To further investigate the DSD variability in Metro Manila, the DSD dataset was categorized into stratiform and convective rainfall type. Stratiform and convective rainfall are different in terms of cloud vertical structure and particle growth processes, hence, their DSD properties were also observed to be distinct (Tokay and Short 1996; Tao et al. 2010). This study implements a rain intensity (R) threshold of 10 mm h^{-1}in classifying stratiform from convective rain types. DSD measurements corresponding to $R < 10$ mm h^{-1} were considered stratiform, while $R \geq 10$ mm h^{-1} were considered convective (Banares et al. 2021). This 10 mm h^{-1} threshold is based on disdrometer, radar, and wind profiler measurements of tropical rainfall over the western pacific (Atlas et al. 1999; Tokay et al. 1999; Ulbrich and Atlas 2007; Sharma et al. 2009).

The mean values of the integral rainfall parameters (IRPs) and the shape (μ) and slope (Λ) parameters for stratiform and convective rainfall are shown in Table 1. Results show that stratiform rains generally have lower values of D_m and higher values of $\text{Log}_{10}\, N_w$ than convective rains. The higher standard deviation (SD) of D_m during convective rains (SD = 0.57) compared to stratiform (SD = 0.28) is a clear function of R, while the higher SD of $\text{Log}_{10}\, N_w$ in stratiform (SD = 0.53) compared to convective rains (SD = 0.38) is due to different microphysical processes (Bringi et al. 2003; Houze 2014). Stratiform clouds with low concentrations of relatively large ice particles aloft result in DSD with relatively lower $\text{Log}_{10}\, N_w$ and larger D_m. In radar observations, stratiform clouds exhibit a pronounced layer of high reflectivity called the bright band. The bright band is the layer where the downwards-settling ice particles start to melt (Yuter and Houze 1997). On the other hand, stratiform clouds with smaller ice particles aloft undergo complete melting (i.e.,

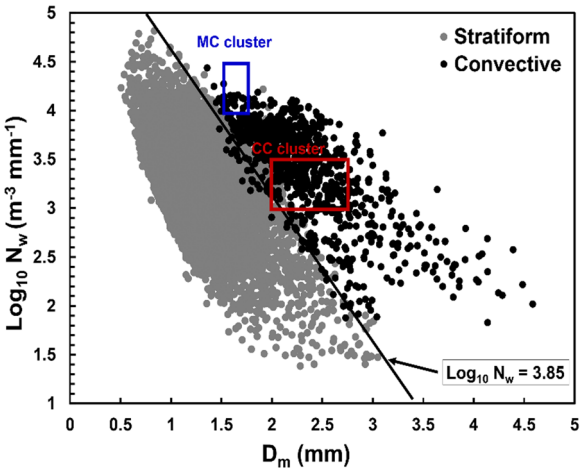

Fig.3 Scatterplot of the D_m vs. $\text{Log}_{10}\, N_w$ values for stratiform (gray circles) and convective (black circles) rains in Metro Manila during the SWM periods of 2020 to 2022. The black solid line represents the convective-stratiform (c-s) separation line proposed by Bringi et al. (2003) while the blue and red boxes denote the maritime convective (MC) and continental convective (CC) clusters respectively

Table 1 Mean of IRPs and gamma parameters during the SWM period in Metro Manila from 2020 to 2022

Rainfall type	Parameters							
	R (mm hr^{-1})	D_m (mm)	$\text{Log}_{10}\, N_w$ (m^{-3} mm^{-1})	N_t (m^{-3})	LWC (g m^{-3})	Z (dBZ)	μ (-)	Λ (mm^{-1})
Stratiform	1.72	1.36	3.10	191.3	0.112	25.2	7.42	9.98
Convective	28.7	2.27	3.36	1049	1.25	45.1	1.55	2.69
Total	5.38	1.53	3.21	301.1	0.26	27.9	6.32	7.50

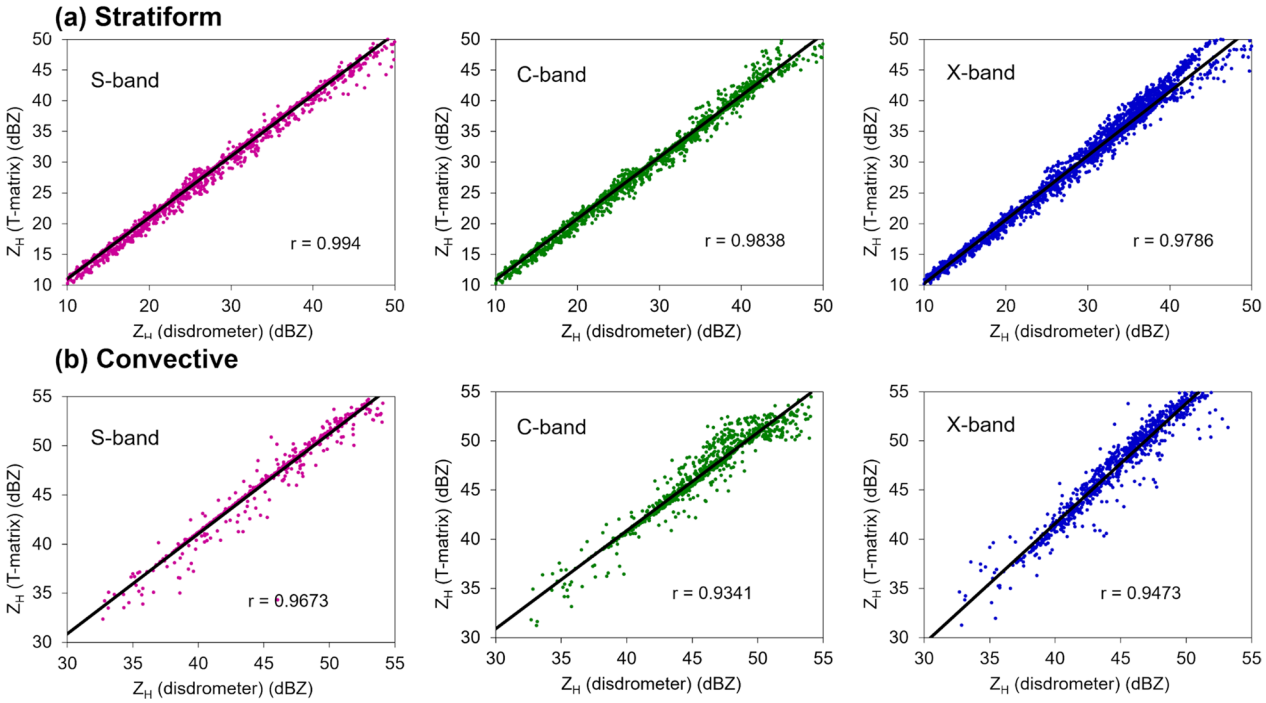

Fig. 4 Comparison between Z_H products of the disdrometer and T-matrix for stratiform and convective rainfall types in Metro Manila

the bright band is not pronounced) before reaching the surface, resulting in DSD with high $\mathrm{Log}_{10} N_w$ and smaller D_m. Both stratiform cloud conditions are present during the SWM period and can be seen in most stratiform rain samples with mid-sized drops (1 mm $< D_m \leq 3$ mm). Figure 3 also shows that the stratiform and convective rain samples during the SWM period in Metro Manila followed the c-s separation line proposed by Bringi et al. (2003). Meanwhile, convective rainfall types are observed to coincide with both maritime (MC) and continental (CC) clusters of Bringi et al. (2003, 2009). This suggests that the microphysical properties of convective rains in Metro Manila are related to both oceanic and continental convection. However, a higher percentage of convective samples fall within the CC cluster more than the MC cluster. This implies that convective rains in Metro Manila during the SWM period, particularly those with larger D_m values ($D_m > 2$ mm), are more continental in terms of origin.

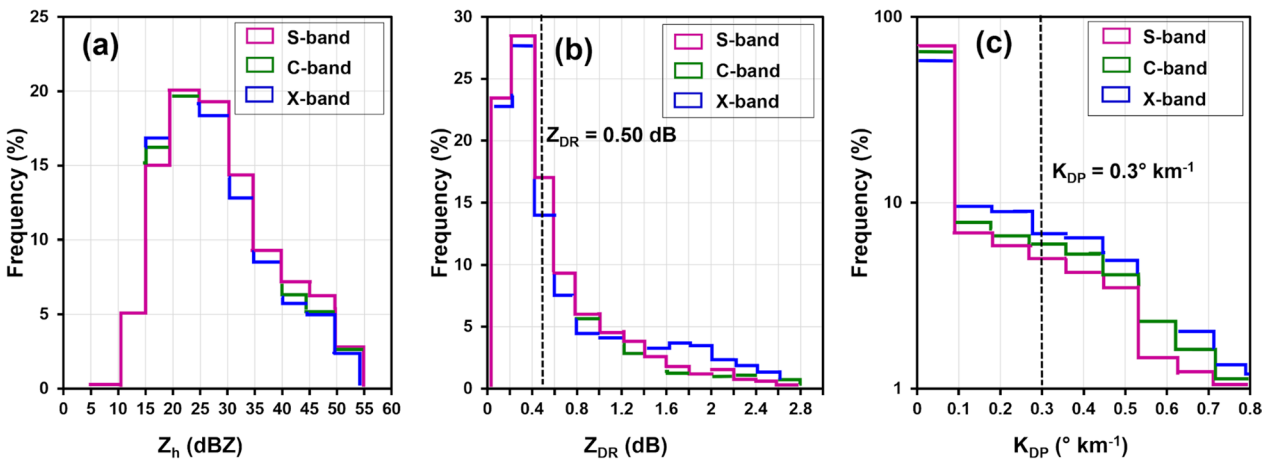

Fig. 5 Frequency distribution of simulated Dual-pol variables using the T-matrix method: (**a**) Z_h, (**b**) Z_{DR}, and (**c**) K_{DP} for Metro Manila during the SWM period. The broken lines in Fig. 4b and c represent Z_{DR} and K_{DP} threshold values proposed by TH18 and C11

3.2 Characteristics of DSD-derived dual-pol variables

The Z_H derived from the disdrometer and the Z_H simulated using the T-matrix method in different radar bands and rain types are compared in Fig. 4. Results show that the disdrometer-derived Z_H shows good agreement with those derived by T-matrix in all radar bands, with r above 0.9. This shows that the T-matrix method is an effective tool for retrieving dual-pol radar parameters from DSD measurements. Figure 5 shows the frequency distribution of simulated Z_H, Z_{DR}, and K_{DP} for different radar bands. The frequency distribution of dual-pol parameters in Fig. 5a shows that the simulated Z_H values did not exceed 60 dBZ in all radar bands. Although S-band moderately had more points at $Z_H \geq 25$ dBZ, all radar bands' mean values are notably close to ~ 29 dBZ. The Z_{DR} peaks at ~ 0.4 dB in all radar bands but is ~ 2–3% higher at $Z_{DR} > 1.4$ dB for X-band (Fig. 5b). The vertical broken lines in Figs. 5b and c depict the threshold values for Z_{DR} and K_{DP} adopted from the study of C11. In the study of TH18, the Z_{DR} threshold was lowered from 0.5 dB to 0.25 dB as they observed that conditions needed to exceed the 0.5 dB threshold were rare for tropical oceanic rains. However, this is not the case in this study since ~ 55% of the simulated Z_{DR} values in all radar bands exceed 0.25 dB. Hence, this study retained the 0.50 dB thresholds for Z_{DR} and 0.3° km^{-1} for K_{DP}. A lower Z_{DR} threshold of 0.5 dB would also increase the utility of Z_{DR} for rainfall estimation while remaining above the accepted noise level ($Z_{DR} > 0.1$ dB; Ryzhkov et al. 2005). ~ 67% of K_{DP} values are found at $K_{DP} < 0.1°$ km^{-1} in all radar bands while higher frequencies are found for X-band at $K_{DP} > 0.1°$ km^{-1}(Fig. 5c). Although a 0.3° km^{-1} threshold for K_{DP} seems restrictive, lowering it is no longer practical for most radar QPE applications because of phase instability (TH18). The 2D histogram plots of simulated dual-pol parameters in Fig. 6 also help visualize the difference between the dual-pol relations and the frequency of when they are utilized for different radar bands. In general, an increase in the use of dual-pol

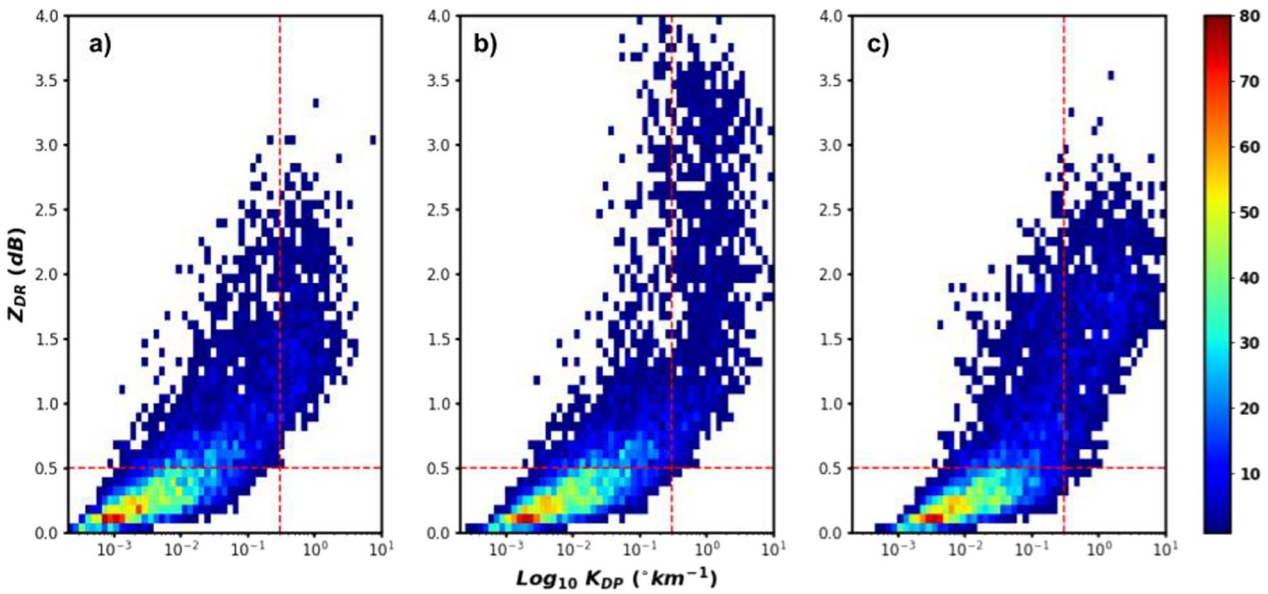

Fig. 6 2D Histogram plot of simulated Z_{DR} and K_{DP} for (**a**) S-band, (**b**) C-band, and (**c**) X-band radar. The red horizontal and vertical broken lines represent the 0.5 dB and 0.3° km^{-1}thresholds for Z_{DR} and K_{DP}, respectively

Table 2 Average values of dual-pol parameters in different radar bands for stratiform, convective, and total rainfall in Metro Manila

Radar bands	S-band			C-band			X-band		
	Dual-pol parameters								
Rainfall type	Z_H (dBZ)	Z_{DR} (dB)	K_{DP} (°km^{-1})	Z_H (dBZ)	Z_{DR} (dB)	K_{DP} (°km^{-1})	Z_H (dBZ)	Z_{DR} (dB)	K_{DP} (°km^{-1})
Stratiform	26.4	0.46	0.024	26.2	0.50	0.050	26.3	0.54	0.083
Convective	46.4	1.35	0.66	46.13	1.76	1.41	48.0	1.66	2.12
Total	29.2	0.58	0.11	29.1	0.67	0.23	29.4	0.69	0.35

parameters (i.e., Z_{DR} and K_{DP}) can be observed with the increase in radar frequency. The bulk of the data points is found in the lower left quadrant of the 2D histogram for all radar bands. By following the blended algorithm of C11, this scenario suggests that $R(Z_H)$ is the most suitable QPE relation for S-band radars. Increased frequency of data points in the upper right quadrant is found for C- and X-band radars (Fig. 6b and c), which

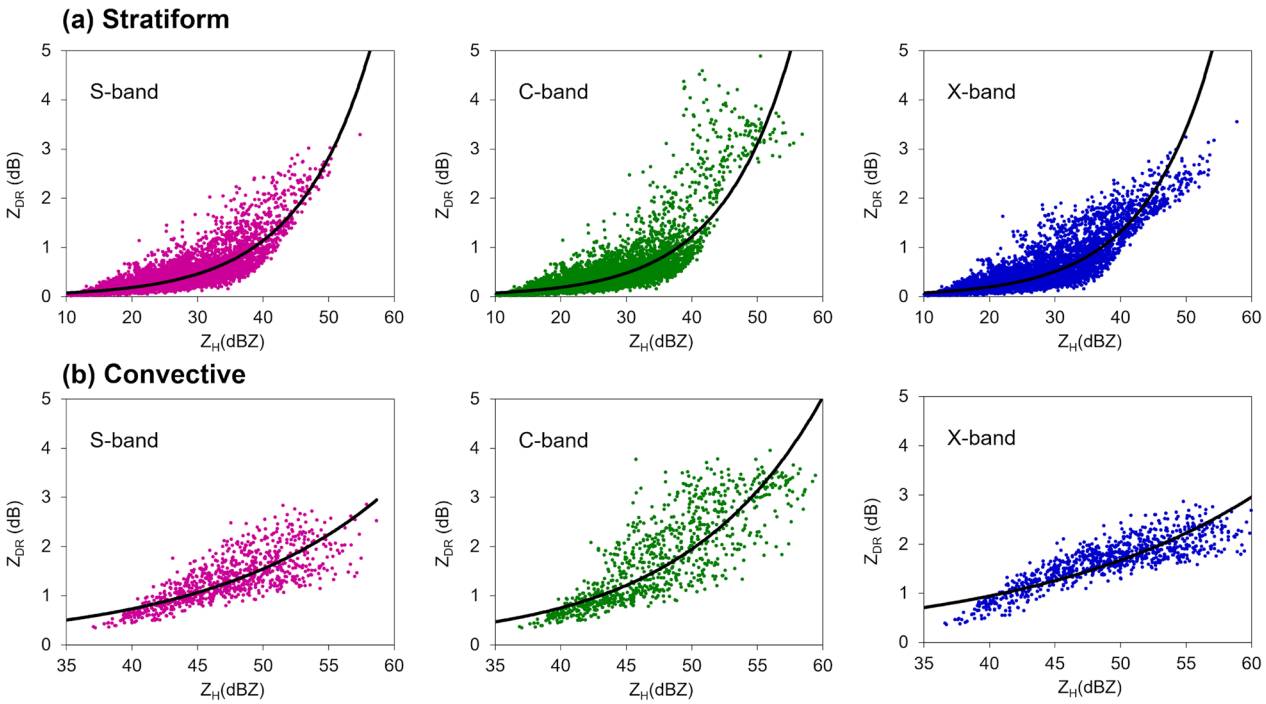

Fig. 7 Z_{DR}—Z_H relations with fitted curves for (**a**) stratiform and (**b**) convective rainfall during the 2020–2022 SWM period in Metro Manila

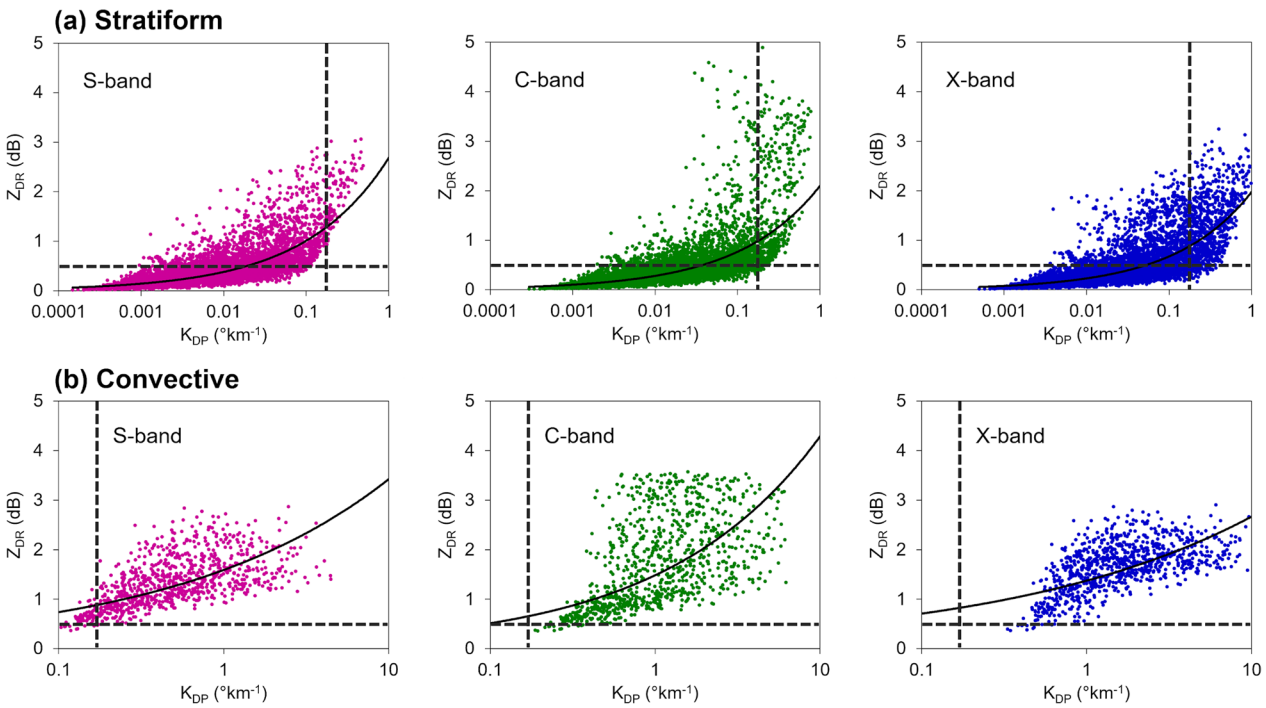

Fig. 8 K_{DP}—Z_{DR} relations with fitted curves for (**a**) stratiform and (**b**) convective rainfall during the 2020–2022 SWM period in Metro Manila

suggests the option for $R(K_{DP})$ and $R(K_{DP}, Z_{DR})$ for QPE. To further elaborate on the effect of DSD variation on the utility of dual-pol relations, the average values of dual-pol variables in different radar bands and rainfall types are shown in Table 2. The average values of Z_H are similar for stratiform (26.4 dBZ) and convective rainfall (46.4 dBZ) in all radar bands except for the X-band which is found to be a little higher during convective rains (48 dBZ).

The average Z_{DR} values for convective rainfall are also higher than stratiform rainfall in all bands. Compared to stratiform rainfall, convective types have higher Z_H, Z_{DR}, and K_{DP}. This demonstrates that raindrops during convective rainfall are relatively larger in size than those of stratiform rainfall, hence the greater difference between Z_H and Z_V which results in larger diameter and more shape deformation. This is also consistent with the larger average D_m of convective rainfall in Table 1. Since K_{DP} is directly related to the liquid water content (*LWC*) and total number concentration (N_t) (Tang et al. 2014), the K_{DP} of convective rainfall is also higher compared to stratiform rainfall in all radar bands. This observation is also consistent with the higher *LWC* and N_t of convective rainfall in Table 1.

The sudden peak of Z_{DR} at $Z_H > \sim 38$ dBZ in stratiform rainfall (Fig. 7a) could be a result of relatively larger raindrops and can also be a suggestive signal of the 38 dBz threshold for stratiform-convective separation regime (Gamache and Houze 1981). For convective rainfall, C-band has the largest Z_{DR} values while a higher percentage of simulated Z_H exceeding 55 dBZ is found for X-band (Fig. 5b). The distribution of the simulated polarimetric variables in Figs. 7 and 8 are also observed to be more dispersed in the C-band, especially for convective rains. The possible reasons for this lie in the DSD properties of convective rains and dependency of the T-matrix simulation on the implemented initial conditions. Zrnić et al. (2000) reported that Z_{DR} and K_{DP} values for C-band radars are highly dependent on the DSD and raindrop temperature, both of which can be extremely variable for convective rains. Additionally, Teschl et al., (2008) showed that resonance effect occurs for raindrop sizes larger than about 5 mm at 5-cm wavelength. Since C-band operates between 4 and 8 cm, the distribution of simulated polarimetric variables, especially K_{DP}, are expected to be noisier. The values of simulated Z_{DR} and Z_H for convective rainfall are found to be more continental in nature, hence the higher magnitude compared to the dominantly oceanic DSD properties in TH18 (Fig. 7b). The differences between maritime and continental DSDs in the tropics can be explained by using the observed differences in the Z_{DR} vs. Z_H distributions. Compared to maritime convection, continental convection has stronger updrafts and more dominant ice microphysical processes, resulting in the formation of graupel and hail that can melt and reach the surface as larger raindrops (Marzuki et al. 2013). Large DSDs with lower N_w would lead to larger Z_H and Z_{DR} (TH18). Moreover, the continental convective cluster of DSDs in the tropics, as defined by Bringi et al. (2003), is more prone to evaporation below the cloud base which can reduce small raindrops and increase the Z_{DR}.

The distribution of Z_{DR} and K_{DP} in Fig. 8 shows that a considerable percentage of both stratiform and convective samples met the 0.50 dB threshold for Z_{DR}. This

Table 3 Dual-pol relations with their corresponding a, b, and c values for different rainfall types and radar bands using the Developed dual-pol relations at S-, C-, and X-bands derived from the DSD measurements for the 2020–2022 SWM period in Metro Manila

		S-band	C-band	X-band
$R(Z_H) = a*Z_H^{\ b}$				
Total rain	a	0.0078	0.0080	0.0083
	b	0.819	0.820	0.827
Convective	a	0.0038	0.454	–
	b	0.649	0.369	–
Stratiform	a	0.0085	0.0086	0.0083
	b	0.801	0.809	0.827
$R(K_{DP}) = a*K_{DP}^{\ b}$				
Total rain	a	40.64	21.33	15.16
	b	0.77	0.87	0.86
Convective	a	40.69	21.13	14.15
	b	0.90	0.90	0.91
Stratiform	a	6.07	7.93	7.97
	b	− 0.26	0.03	0.14
$R(Z_H, Z_{DR}) = a*Z_H^{\ b}Z_{DR}^{\ c}$				
Total rain	a	0.000074	0.0056	0.0038
	b	0.98	0.75	0.803
	c	− 1.34	− 1.34	− 1.44
Convective	a	0.00035	0.00055	–
	b	0.833	0.810	–
	c	− 1.02	− 0.54	–
Stratiform	a	0.0001	0.00063	0.00038
	b	0.94	0.73	0.80
	c	-1.39	− 1.30	− 1.43
$R(K_{Dp}, Z_{DR}) = a*K_{DP}^{\ b}Z_{DR}^{\ c}$				
Total rain	a	62.65	27.05	21.83
	b	0.96	0.95	0.99
	c	− 1.068	− 0.464	− 0.884
Convective	a	59.19	26.36	21.00
	b	0.99	0.97	1.00
	c	− 0.91	− 0.42	− 0.79
Stratiform	a	45.53	9.76	10.26
	b	0.08	0.11	0.32
	c	− 1.89	− 0.20	− 0.37

motivates the option to use $R(Z_H, Z_{DR})$ for QPE. However, most stratiform DSD samples did not meet the 0.3° km^{-1} K_{DP} threshold, especially for the S-band (Fig. 8a). Furthermore, Fig. 8 also illustrates that DSD samples with $K_{DP} > 0.3°\ km^{-1}$ are always associated with $Z_{DR} > 0.5$ dB in all radar bands and rain types. Similar observations were reported in TH18, but for a lower threshold of $Z_{DR} > 0.25$ dB. The distribution of simulated dual-pol variables and the Z_{DR} and K_{DP} thresholds suggest that $R(Z_H)$ and $R(Z_H, Z_{DR})$ relations are for stratiform rain types ($R < 10$ mm h^{-1}), while $R(K_{DP})$ or $R(K_{DP}, Z_{DR})$ can be utilized for convective rain types ($R \geq 10$ mm h^{-1}).

3.3 Evaluation of derived dual-polarimetric relations

Results discussed in Sect. 3.2 clearly demonstrated the applicability of dual-pol parameters on QPE differs for different DSD properties and radar bands. Table 3 presents the derived dual-pol relations for different radar bands and rain types during the SWM period in Metro Manila. It can be observed that coefficient a in $R(K_{DP})$ and $R(K_{DP}, Z_{DR})$ are larger compared to $R(Z_H)$ and $R(Z_H, Z_{DR})$ in all radar frequencies and rainfall types. The coefficient a in $R(K_{DP})$ and $R(K_{DP}, Z_{DR})$ derived from the total rainfall decreases as the radar frequency increases from S-band to X-band, while the coefficient c has a negative value for all rainfall types in order to constrain the positive correlation of Z_H and K_{DP} to R (TH18). It can also be noticed that there were no derived $R(Z_H)$ and $R(Z_H, Z_{DR})$ relations for convective rainfall in X-band. This is due to the implementation of K_{DP} and Z_{DR} thresholds of C11 and TH18 as discussed in Sect. 3.2. In comparison with MC21, the $R(K_{DP})$ obtained in this study have similar values of a but slightly higher values of b compared to MC21 ($a = 21.18$, $b = 0.71$). In terms of $R(Z_H, Z_{DR})$, MC21 reported a relatively lower value of a, and higher values of b and c ($a = 0.0025$, $b = 0.9340$, $c = -0.86$). Finally, the $R(K_{DP}, Z_{DR})$ found in this study also has similar b but different a and c values compared to MC21 ($a = 31.27$, $b = 0.95$, $c = -0.70$). The differences in the obtained dual-pol relations in Metro Manila and Southern Luzon show distinct DSD properties between the two regions despite being affected by a similar synoptic system during the SWM period. These observations also show the need to implement localized QPE relations for Metro Manila.

Rainfall data from the Science Gardena and La Mesa watershed disdrometer stations were used to evaluate the performance of the relationships. For this section and the succeeding discussions, the dual-pol relations will have the subscripts TOT, STR, and CNV which correspond to the derived relationships for the total, stratiform, and

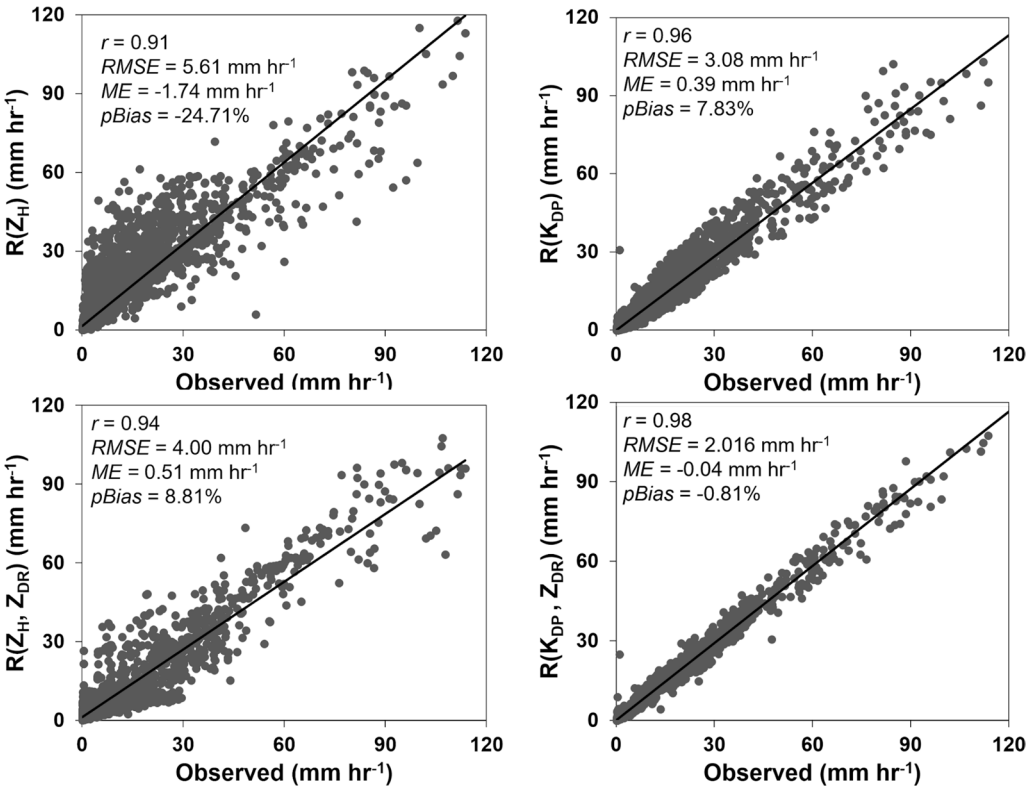

Fig. 9 Scatterplots of rain rate estimates from the C-band relations for the total rainfall during the SWM period in Metro Manila. The correlation coefficient (*r*), root mean square error (*RMSR*), mean error (*ME*), and percent bias (*pBias*) are also included

convective rainfall, respectively. The scatterplots of the observed rain rates with those derived from the dual-pol relationships for the C-band radar are shown in Fig. 9. A significant improvement in the statistics was observed when the relationship was change from the classic $R(Z_H)$ to $R(Z_{DR})$ and $R(K_{DP})$ or a combination of K_{DP} and Z_{DR}. The same improvements were observed for the S- and X-band but were not shown here. $R(K_{DP})_{TOT}$ and $R(K_{DP}, Z_{DR})_{TOT}$ significantly reduced the ME and RMSE when compared to $R(Z_H)_{TOT}$ which suggests that the relationship between R and K_{DP} is more linear in nature. Furthermore, $R(K_{DP}, Z_{DR})_{TOT}$ statistically outperformed the other dual-pol relation and shows that a multiparameter relation can significantly lower the errors and biases in the rainfall estimates. To evaluate the performance of the derived dual-pol relations in generating QPEs, two continuous rain events in Metro Manila during the study period were chosen as test cases. For future operational purposes, only the dual-pol relations derived for the C-band Radar will be evaluated in the next sub-sections since the nearest dual-pol Radar in Metro Manila operates within the C-band. The performance of each dual-pol relation is discussed in the succeeding sub-sections.

3.3.1 Event 1: 24 June 2021 heavy rainfall

Event 1 was recorded by the Science Garden disdrometer station and lasted for ~ 2 h with an average R of 8.58 mm h^{-1}. The highest R were recorded between 12:05–12:30 UTC and 13:20–13:45 UTC with maximum values of 33.6 mm h^{-1} and 42 mm h^{-1}, respectively. The average mass-weighted mean diameter (D_m) recorded during the entire event was 1.83 mm. Figure 10 shows the time series and scatter plots of R derived from the Science Garden disdrometer station and from the dual-pol relations. The standard Marshall & Palmer ($R(Z_{MP})$) relation ($Z = 200R^{1.6}$) was also used for comparison. The time series shows similar troughs and peaks throughout the rain event (Fig. 10a). However, large discrepancies

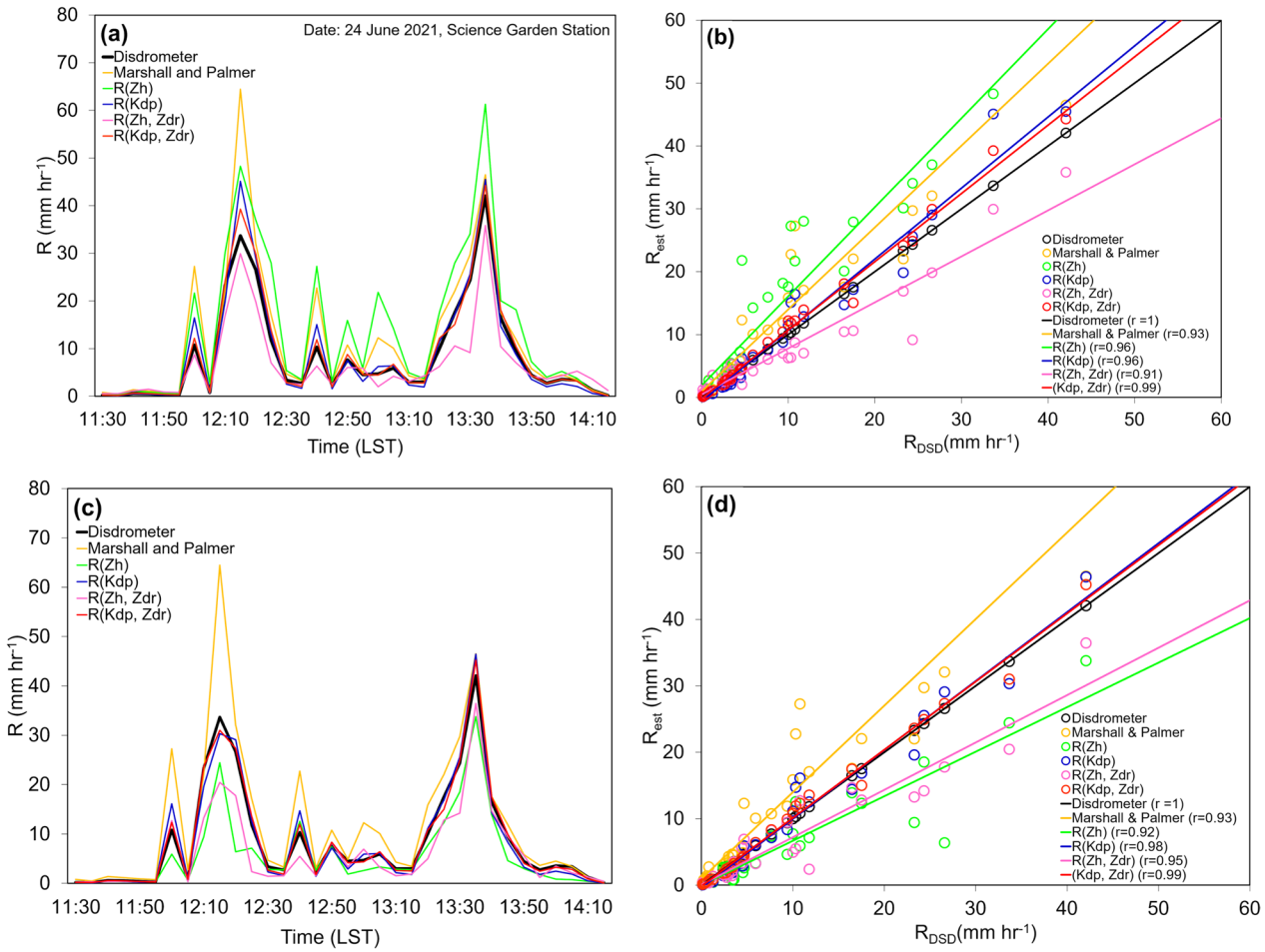

Fig. 10 Comparison between the time series and scatter plots of R derived using the Marshall & Palmer relation ($Z = 200R^{1.6}$) and the C-band dual-pol relations. **a** and **b** show the time series and scatterplot of derived R using the dual-pol relations for the total rainfall, while **c** and **d** show the derived R using the dual-pol relations for convective rainfall

were observed during high rain rate periods between 12:00–12:30 UTC and 13:10–13:50 UTC. $R(Z_{MP})$ and $R(Z_H)_{\mathrm{Tot}}$ generally overestimate rainfall with a pBias of (+)29% and (+)39%, respectively. Meanwhile, $R(Z_H, Z_{DR})_{\mathrm{TOT}}$ is observed to underestimate rainfall by (−)27%. Among the relationships, $R(K_{DP})_{\mathrm{TOT}}$ and $R(K_{DP}, Z_{DR})_{\mathrm{TOT}}$ performed relatively better compared with other dual-pol relations, with r values of 0.96 and 0.99, respectively (Fig. 10 b). $R(K_{DP})_{\mathrm{TOT}}$ and $R(K_{DP}, Z_{DR})_{\mathrm{TOT}}$ also statistically outperform all other Z_H-based QPEs in terms of RMSE [2.63 mm h^{-1} and 1.48 mm h^{-1}, respectively], ME [0.49 mm h^{-1} and 0.58 mm h^{-1}, respectively], and pBias [(+)5.43% and (+)6.32%, respectively]. Since Event 1 is a heavy rainfall event, the QPE products of dual-pol relations for convective rain are also evaluated in Fig. 10c and d. Results show that both $R(Z_H)_{\mathrm{C}}$ and $R(Z_H, Z_{DR})_{\mathrm{C}}$ generally underestimated the rainfall, while $R(K_{DP})_{\mathrm{CNV}}$ and $R(K_{DP}, Z_{DR})_{\mathrm{CNV}}$ outperformed all dual-pol QPEs. In fact, $R(K_{DP})_{\mathrm{CNV}}$ and $R(K_{DP}, Z_{DR})_{\mathrm{CNV}}$ performed better than $R(K_{DP})_{\mathrm{TOT}}$ and $R(K_{DP}, Z_{DR})_{\mathrm{TOT}}$ in terms of all the statistical validation parameters. This can be easily observed by comparing the fitted lines of $R(K_{DP})_{\mathrm{T}}$ and $R(K_{DP}, Z_{DR})_{\mathrm{T}}$ in Fig. 10b to the linear regression fit of $R(K_{DP})_{\mathrm{C}}$ and $R(K_{DP}, Z_{DR})_{\mathrm{C}}$ in Fig. 11b. $R(K_{DP})_{\mathrm{CNV}}$ and $R(K_{DP}, Z_{DR})_{\mathrm{CNV}}$ also significantly reduced the RMSE [1.9 mm h^{-1} and 1.05 mm h^{-1}, respectively], ME [-0.097 mm h^{-1} and 0.059 mm h^{-1}, respectively], and pBias [(−)1.14% and (+)0.68%, respectively] compared to $R(K_{DP})_{\mathrm{TOT}}$ and $R(K_{DP}, Z_{DR})_{\mathrm{TOT}}$.

3.3.2 Event 2: 19 July 2021 stratiform rain

Event 2 was recorded by the La Mesa watershed disdrometer station. The rainfall event lasted for ~ 3 h and 30 min. with an average R of 1.5 mm h^{-1}. The maximum $R = 7.97$ mm h^{-1} was observed at the beginning of the rain event around 17:15 UTC. The average mass-weighted mean diameter (D_m) recorded during the entire event was

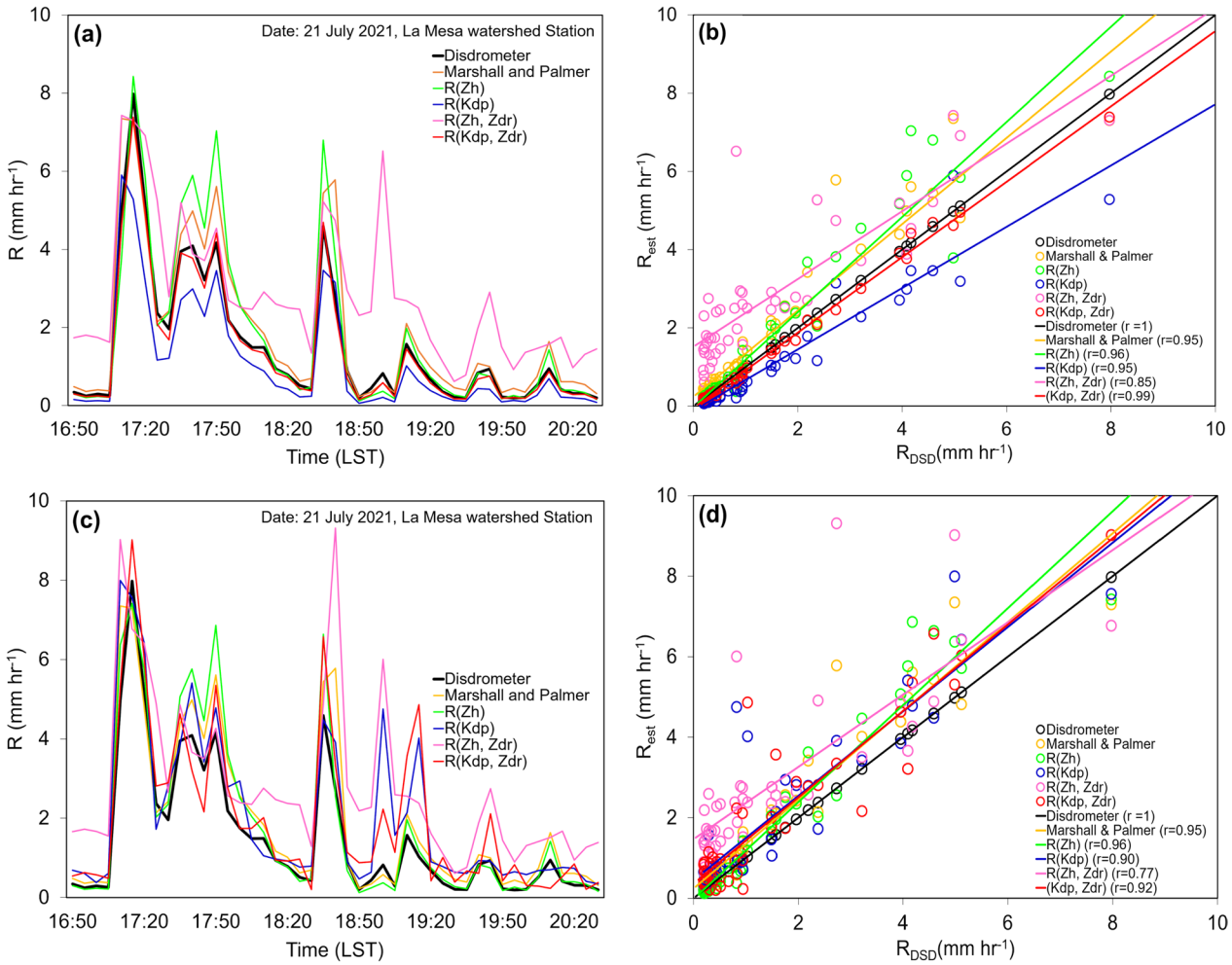

Fig. 11 Comparison between the time series and scatter plots of R derived using the Marshall & Palmer relation ($Z = 200R^{1.6}$) and the C-band dual-pol relations. **a** and **b** show the time series and scatterplot of derived R using the dual-pol relations for the total rainfall, while **c** and **d** show the derived R using the dual-pol relations for stratiform rainfall

1.23 mm. Compared to Fig. 10a, $R(Z_H)_{TOT}$ performed relatively better in stratiform than convective rainfall events. Although $R(Z_H)_{TOT}$ has a slight overestimation, it still has lower pBias [(+)16%] and ME (0.29 mm h^{-1}) compared to the $R(Z_{MP})$ [pBias = (+)21%, ME = 0.4 mm h^{-1})]. On the other hand, $R(Z_H, Z_{DR})_{TOT}$ performed relatively better in Event 1 than here in Event 2 as it generally overestimated R having an RMSE = 1.62 mm h^{-1} and pBias = (+)46.7%. $R(K_{DP})_{TOT}$ also performed relatively poorer here in Event 2 and underestimated R (Fig. 11b) having a pBias = (−)42% and ME = -0.44 mm h^{-1}. $R(K_{DP}, Z_{DR})_{TOT}$ statistically outperformed the other dual-pol relations having the lowest RMSE = 0.16 mm h^{-1}, ME = -0.1 mm h^{-1} and pBias = − 7.4%. $R(K_{DP}, Z_{DR})_{TOT}$ was able to capture the rainfall peaks better compared to the other dual-pol relations. $R(Z_H)_{STR}$ provided the best statistics in Fig. 11c and d in terms of the stratiform dual-pol relations. Similar to Fig. 11a, $R(K_{DP})_{STR}$, $R(Z_H, Z_{DR})_{STR}$, and $R(K_{DP}, Z_{DR})_{STR}$ failed to capture most of the rainfall peaks and overestimated R. $R(Z_H)_{STR}$ also outperformed $R(Z_{MP})$ in terms of lower RMSE, ME, and pBias. The results presented in Events 1 and 2 show that K_{DP} and Z_{DR} can provide a more accurate QPE under heavy rain conditions compared to Z_H, while Z_H can still be considered a better estimator for light rains compared to $R(Z_{MP})$. All in all, $R(K_{DP}, Z_{DR})$ has the best performance in both convective and stratiform rain events. These findings agree with other dual-pol studies that $R(K_{DP})$ and $R(K_{DP}, Z_{DR})$ result in better rainfall estimates compared to conventional single-parameter relations (Chen et al. 2017; Voormansik et al. 2020) and further prove the effectivity of the threshold-based utilization of K_{DP} and Z_{DR} in C11 and TH18.

4 Summary and conclusion

In this study, the three-year worth of DSD data collected from the Science Garden and La Mesa watershed disdrometer stations during the Southwest monsoon (SWM) period were used to investigate the microphysical characteristics of rainfall in Metro Manila and develop QPE relations for S-, C-, and X-band dual-polarimetric radars. The DSD characteristics during the SWM period are discussed and the performance of the QPE relations is also evaluated. The major conclusions are as follows.

1 The observed DSD characteristics in Metro Manila show higher variability in terms of raindrop sizes compared to neighboring countries and regions (Seela et al. 2017). The smaller values of μ and Λ parameters in Metro Manila during the SWM period also indicate that despite the similarities in D_m and N_w values in Southern Luzon (Macuroy et al. 2021), Metro Manila DSD is still more distributed to larger raindrops. A clear distinction between the DSD properties of stratiform and convective rainfall was also observed. The stratiform and convective DSD samples during the SWM period follow the convective-stratiform separation line of Bringi et al. (2003) and suggest that the microphysical processes of convective rainfall in Metro Manila during the SWM period are influenced by both continental and maritime convection.

2 The derived Z_H values using the T-matrix scattering method have good agreement with the DSD-derived Z_H values, thus showing that the T-matrix is an effective method in simulating dual-pol parameters using disdrometer measurements. In all radar bands, the simulated Z_H values for the total rainfall in Metro Manila during the SWM period did not exceed 60 dB. Moreover, 55% of simulated Z_{DR} were also found to be less than 0.25 dB, and 67% of K_{DP} values were less than 0.1° km^{-1}. Meanwhile, $Z_{DR} > 1.4$ dB and $K_{DP} > 0.1°$ km^{-1} are found to have higher frequencies in X-band. In terms of rainfall type, the average value of Z_H of convective rains is found to be the same for S- and C-band (46.4 dBZ) but slightly higher for X-band (48 dBZ).

3 The distribution of the dual-pol parameters among different radar bands and rain types shows that there is a need to implement certain data quality thresholds to determine the usability of a certain dual-pol relation. The 0.5 dB and 0.3° km^{-1} thresholds for Z_{DR} and K_{DP} based on the blended algorithm of C11 and TH18 show that dual-pol relations involving Z_{DR} and K_{DP} are recommended to be used especially for C- and X-band. Localized dual-pol estimators such as $R(Z_H)$, $R(K_{DP})$, $R(Z_H, Z_{DR})$, and $R(Z_{DR}, K_{DP})$ were also developed by applying the thresholds to the simulated dual-pol parameters. In general, the localized dual-pol relations can decrease the RMSE and ME by at least 7.43% and 30.25%, respectively relative to the conventional $R(Z_{MP})$. Evaluation of the QPEs from the dual-pol relations for the C-band radar shows that $R(Z_H)$ is most sensitive to DSD variations hence its poor performance, especially during convective rains. Moreover, according to MC21, $R(Z_H)$ and $R(Z_H, Z_{DR})$ relations are more sensitive to the number of small raindrops than the proportion of large raindrops. Hence, these two rainfall estimators are not recommended for convective rain types since they contain higher concentrations of large raindrops compared to stratiform rain types. On the other hand, the relatively good performance of $R(K_{DP})$ and $R(K_{DP}, Z_{DR})$ can be attributed to their lesser sensitivity to DSD variation compared to Z_H (Zhang et al.

2019) and to the immunity of K_{DP} to radar attenuation and calibration (MC21).

The comprehensive analysis of DSD properties is an important step in developing localized QPE relations since variation in the DSD is one of the major sources of error in radar QPE products. Hence, this study investigated the DSD characteristics of rainfall in Metro Manila during the SWM period using DSD measurements from two PARSIVEL^2 disdrometer stations. The study also introduced an effective method of developing dual-pol relations for S-, C-, and X-band radars using DSD measurements. Since this study is focused on the performance of the QPE products in C-band radar only, other dual-pol relations mentioned in this study can be further evaluated for S- and X-band. The DSD properties observed in this study, together with the derived localized QPE relations do not necessarily reflect the DSD characteristics and dual-pol relations of other monsoon seasons and locations in the Philippines. Nevertheless, the results presented in this study, especially the derived dual-pol relations, can provide possible improvements in the general rainfall retrieval operations of the country's dual-pol and single-pol radar networks.

Appendix

See Fig. 12 and Table 4.

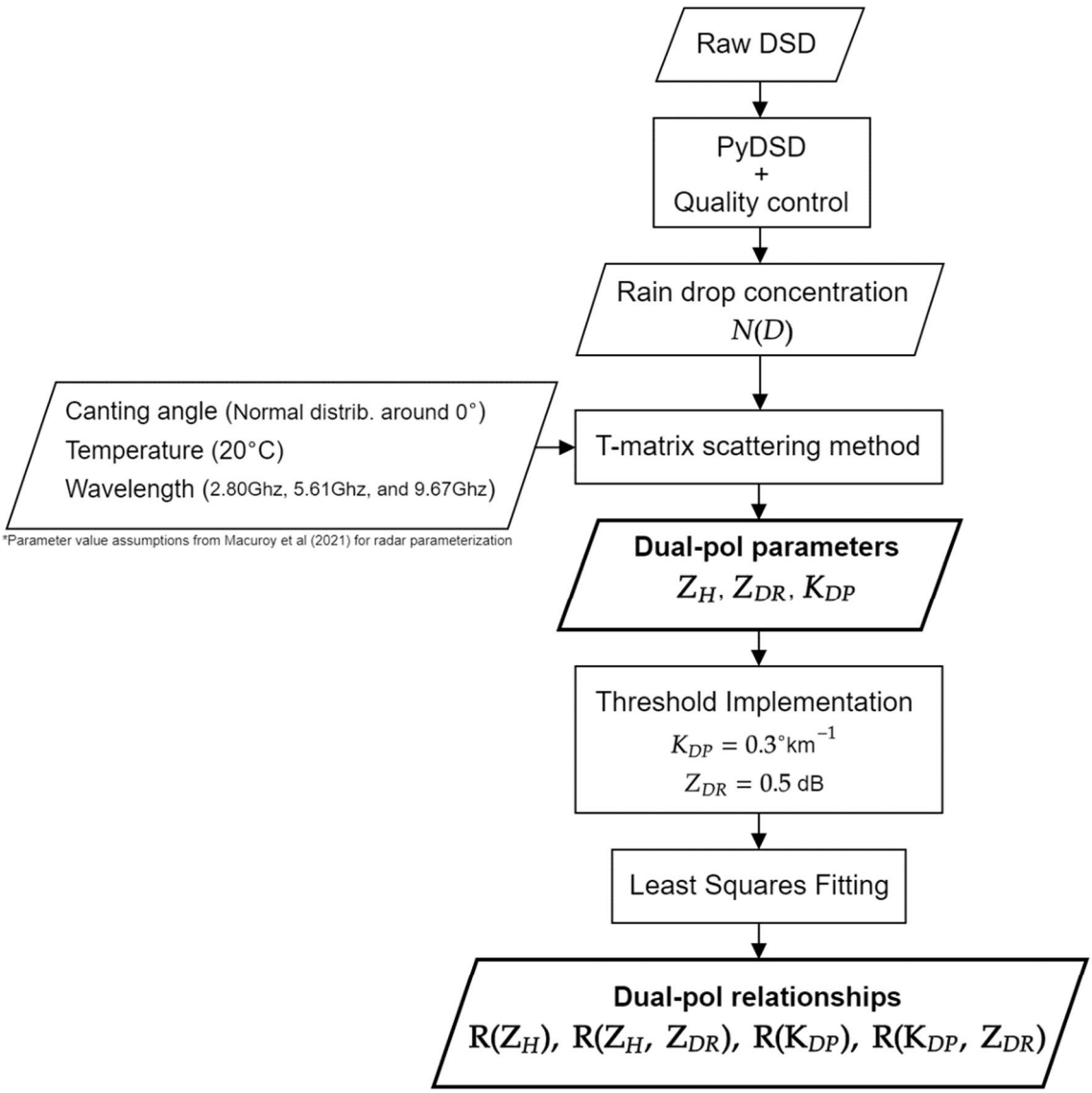

Fig. 12 Process flow of T-matrix from the PyDSD package for simulating the dual-pol parameters and relations from the DSD measurements

Table 4 Drop size distribution class bins of the PARSIVEL^2 optical Disdrometer

Class number	Classification of drops according to volume-equivalent diameter		Classification of drops according to fall velocity	
	Class average (mm)	Class spread (mm)	Class average (mm s^{-1})	Class spread (mm s^{-1})
1	0.062	0.125	0.050	0.1
2	0.187	0.125	0.150	0.1
3	0.312	0125	0.250	0.1
4	0.437	0.125	0.350	0.1
5	0.562	0.125	0.450	0.1
6	0.687	0.125	0.550	0.1
7	0.812	0.125	0.650	0.1
8	0.937	0.125	0.750	0.1
9	1.062	0.125	0.850	0.1
10	1.187	0.125	0.950	0.1
11	1.375	0.250	1.1	0.2
12	1.625	0.250	1.1	0.2
13	1.875	0.250	1.5	0.2
14	2.125	0.250	1.7	0.2
15	2.375	0.250	1.9	0.2
16	2.750	0.5	2.2	0.4
17	3.250	0.5	2.6	0.4
18	3.750	0.5	3	0.4
19	4.250	0.5	3.4	0.4
20	4.750	0.5	3.8	0.4
21	5.5	1	4.4	0.8
22	6.5	1	5.2	0.8
23	7.5	1	6	0.8
24	8.5	1	6.8	0.8
25	9.5	1	7.6	0.8
26	11	2	8.8	1.6
27	13	2	10.4	1.6
28	15	2	12	1.6
29	17	2	13.6	1.6
30	19	2	15.2	1.6
31	21.5	3	17.6	3.2
32	24.5	3	20.8	3.2

Acknowledgements
This research is funded by the Department of Science and Technology, Philippine Council for Industry, Energy and Emerging Technology Research Development (DOST-PCIEERD) under the Manila Economic and Cultural Office – Taipei Economic and Cultural Office (MECO-TECO) Volcano, Ocean, Typhoon, and Earthquake (VOTE) Initiative. The authors would also like to acknowledge the Philippines Atmospheric, Geophysical and Astronomical Services Administration (PAGASA) for the provision of the Disdrometer and Automated weather station data and for providing additional support for this study.

Author contributions
Conceptualization, MPI, SCM, AGP; Methodology, MPI and SCM; Formal analysis, MPI & SCM; Visualization; SCM, MPI, and RAS; Data acquisition, RAS, MPI, and SCM; Data curation, SCM, MPI, and RAS; Funding acquisition, EOC and AGP; Project Administration, AGP and EOC; Supervision, W-YC and BJ-DJ; Writing—original draft, MPI; Review and editing, all authors.

Data availability
Figure 1 was generated using available terrain shapefiles from ArcMap. The PyDSD processing codes are available through J. Hardin at https://github.com/josephhardinee/PyDSD and at Hardin (2014) under the doi: https://doi.org/https://doi.org/10.5281/zenodo.9991.

Declarations

Competing interests
The authors declare that they have no competing interests.

Author details
[1]Philippine Atmospheric, Geophysical, and Astronomical Services Administration, Science Garden Compound, Senator Miriam P. Defensor-Santiago Avenue, 1100 Quezon City, Philippines. [2]Department of Atmospheric Science, National Taiwan University, Taipei 10617, Taiwan. [3]Department of Atmospheric Sciences, National Central University, Taoyuan 32001, Taiwan.

Received: 7 March 2023 Accepted: 4 December 2023
Published online: 18 December 2023

References

Angulo-Martinez M, Begueria S, Latorre B, Fernandez-Raga M (2018) Comparison of precipitation measurements by OTT Parsivel^2 and Thies LPM optical disdrometers. Hydrol Earth Syst Sci 22:2811–2837. https://doi.org/10.5194/hess-22-2811-2018

Asuncion JF, Jose AM (1980) A study of the characteristics of the northeast and southwest monsoon in the Philippines. National Research Council of the Philippines Assisted Project.

Atlas D, Ulbrich CW, Marks FD Jr, Amitai E, Williams CR (1999) Systematic variation of drop size and radar-rainfall relations. J Geog Res 104:6155–6169. https://doi.org/10.1029/1998JD200098

Bagtasa G (2019) Enhancement of summer monsoon rainfall by tropical cyclones in northwestern Philippines. J Meteorol Soc Japan 97(5):967–976. https://doi.org/10.2151/jmsj.2019-052

Banares EN, Narisma GT, Simpas JB, Cruz FT, Lorenzo GR, Cambaliza MO, Coronel RC (2021) Seasonal and diurnal variations of observed convective rain events in Metro Manila, Philippines. Atmos Res 258:105646. https://doi.org/10.1016/j.atmosres.2021.105646

Beard KV (1976) Terminal velocity and shape of cloud and precipitation drops aloft. J Atmos Sci 33:851–864. https://doi.org/10.1175/1520-00469(1976)033%3c0851:TVASOC%3e2.0.co;2

Brandes EA, Zhang G, Vivekanandan J (2002) Experiments in rainfall estimation with a polarimetric radar in a subtropical environment. J Appl Meteor 41:674–685. https://doi.org/10.1175/1520-0450(2002)041%3c0674:EIREWA%3e2.0CO;2

Bringi VN, Chandrasekar V, Hubbert J, Gorgucci E, Randeu WL, Schoenhuber M (2003) Raindrop size distribution in different climatic regimes from disdrometer and dual-polarized radar analysis. J Atmos Sci 60:354–365. https://doi.org/10.1175/1520-0469(2003)060%3c0354:RSDIDC%3e2.0.co;2

Bringi VN, Williams CR, Thurai M, May PT (2009) Using dual-polarized radar and dual-frequency profiler for DSD characterization: a case study from Darwin, Australia. J Atmos Ocean Technol 26:2107–2122. https://doi.org/10.1175/2009JTECHA1258.1

Cayanan EO, Chen T-C, Argete JC, Yen M-C, Nilo PD (2011) The effect of tropical cyclone on southwest monsoon rainfall in the Philippines. J Meteorol Soc Japan 89A:123–139. https://doi.org/10.2151/jmsj.2011-A08'

Chen G, Zhao K, Zhang G, Huang H, Liu S, Wen L, Yang Z, Yang L, Xu L, Zhu W (2017) Improving polarimetric C-band radar rainfall estimation with two-dimensional video disdrometer observations in Eastern China. J Hydrometeorol 18:1375–1391. https://doi.org/10.1175/JHM-D-16-0215.1

Cifelli R, Chandrasekar V, Lim S, Kennedy PC, Wang Y, Rutledge SA (2011) A new dual-polarization radar rainfall algorithm: application in Colorado

precipitation events. J Atmos Ocean Technol 28:352–364. https://doi.org/10.1175/2010JTECHA1488.1
Crisologo I, Vulpiani G, Abon CC, David CPC, Bronstert A, Heistermann M (2014) Polarimetric rainfall retrieval from a C-band weather radar in a tropical environment (The Philippines). Asia-Pac J Atmos Sci 50:595–607. https://doi.org/10.1007/s13143-014-0049-y
Cruz FT, Narisma GT, Villafuerte MQ II, Cheng Chua KU, Olaguera LMP (2013) A climatological analysis of the southwest monsoon rainfall in the Philippines. Atmos Res 122:609–616. https://doi.org/10.1016/j.atmosres.2012.06.010
Gamache JF, Houze RA (1981) The water budget of a tropical squall-line system. In conference on radar meteorology, 20th, Boston, MA 346–352
Hachani S, Boudevillain B, Delrieu G, Bargaoui Z (2017) Drop size distribution climatology in Cevennes-Vivarais Region. France Atmosphere 8:233. https://doi.org/10.3390/atmos8120233
Hardin J (2014) PyDisdrometer v1.0. Zenodo. https://doi.org/10.5281/zenodo.9991
Heistermann M, Crisologo I, Abon CC, Racoma BA, Jacobi S, Servando NT, David CPC, Bronstert A (2013) Brief communication "using the new Philippines radar network to reconstruct the Habagat of August 2012 monsoon event around Metropolitan Manila." Nat Hazards Earth Syst Sci 13:653–657. https://doi.org/10.5194/nhess-13-653-2013
Houze Jr. RA (2014) Chapter 3 Cloud Microphysics. International Geophysics, Academic Press. Elsevier 104. 47–76
Ibanez MP, Pura AG, Sajulga RA, David SJ (2023) Raindrop size distribution (RSD) characteristics during the southwest monsoon period in Western Luzon. Philipp J Sci 152(S1):1–16
Jamandre CA, Narisma GT (2013) Spatio-temporal validation of satellite-based rainfall estimates in the Philippines. Atmos Res 122:599–608. https://doi.org/10.1016/j.atmosres.2012.06.024
Janapati J, Seela BK, Lin P-L, Wang PK, Tseng CH, Reddy KK, Hashiguchi H, Feng L, Das SK, Unikrishnan CK (2021) Raindrop size distribution characteristics of Indian and Pacific Ocean tropical cyclones observed at India and Taiwan sites. J Meteorol Soc Japan 98:299–317. https://doi.org/10.2151/jmsj.2020-015
Ji L, Chen H, Li L, Chen B, Xiao X, Chen M, Zhang G (2019) Raindrop size distribution and rain characteristics observed by a PARSIVEL disdrometer in Beijing, Northern China. Remote Sens 11(12):1479. https://doi.org/10.3390/rs11121479
Krishna UVM, Reddy KK, Seela BK, Shirooka R, Lin PL, Pan CJ (2016) Raindrop size distribution of easterly and westerly monsoon precipitation observed over Palau islands in the Western Pacific Ocean. Amos Res 174–175:41–51. https://doi.org/10.1016/j.atmosres.2016.01.013
Lee M, Kang N, Joo H, Kim HS, Kim S, Lee J (2019) Hydrological modeling approach using radar-rainfall ensemble and multi-runoff-model blending technique. Water 11:850. https://doi.org/10.3390/w11040850
Loffler-Mang M, Joss J (2000) An optical disdrometer for measuring the size and velocity of hydrometeors. J Atmos Oceanic Technol 17:130–139. https://doi.org/10.1175/1520-0426(1948)005%3c0165:TDORWS%3e2.0.co;2
Macuroy JT, Chang W-Y, Faustino-Eslava DV, Sanchez PAJ, Tiburan CL Jr, Jou BJ-D (2021) Evaluations on radar QPE using raindrop size distribution in Southern Luzon, Philippines. Terr Atmos Ocean Sci 32:693–724. https://doi.org/10.3319/TAO.2021.02.22.01
Marshall JS, Palmer WMK (1948) The distribution of raindrops with size. J Meteorol 5:165–166. https://doi.org/10.1175/1520-0469(1948)005%3c0165:tdorws%3e2.0.co;2
Marzuki M, Hashiguchi H, Yamamoto MK, Mori S, Yamanaka MD (2013) Regional variability of raindrop size distribution over Indonesia. Ann Geophys 31:1941–1948. https://doi.org/10.5194/angeo-31-1941-2013
Matsumoto J, Olagueara LMP, Nguyen-Le D, Kubota H, Villafuerte MQ II (2020) Climatological seasonal changes of wind and rainfall in the Philippines. Int J Climatol 40:4843–4857. https://doi.org/10.1002/joc.6492
Mishchenko MI, Travis LD, Macke A (1996) Scattering of light by polydisperse, randomly oriented, finite circular cylinders. Appl Opt 35:4927–4940
Rosenfeld D, Wolff DB, Atlas D (1993) General probability-matched relations between radar reflectivity and rain rate. J Appl Meteorol 32:50–72. https://doi.org/10.1175/1520-0450(1993)032%3c0050:GPMRBR%3e2.0.co;2
Ryzhkov AV, Giangrande SE, Melnikov VM, Schue TJ (2005) Calibration issues of dual-polarization radar measurements. J Atmos Ocean Technol 22:1138–1155. https://doi.org/10.1175/JTECH1772.1
Seela BK, Janapati J, Lin P-L, Reddy KK, Shirooka R, Wang PK (2017) A comparison study of summer season raindrop size distribution between Palau and Taiwan, two islands in Western Pacific. J Geophys Res 122:11787–21180. https://doi.org/10.1002/2017JD026816
Seela BK, Janapati J, Lin P-L, Wang PK, Lee MT (2018) Raindrop size distribution characteristics of summer and winter season rainfall over north Taiwan. J Geophys Res Atmos 123:11602–11624. https://doi.org/10.1029/2018JD028307
Seliga TA, Bringi VN (1976) Potential use of radar differential reflectivity measurements at orthogonal polarizations for measuring precipitation. J Appl Meteorol Climatol 15:69–76. https://doi.org/10.1175/1520-0450(1976)015%3c0069:PUORDR%3e2.0.co;2
Sharma SM, Konwar M, Sarma DK, Kalapureddy MCR, Jain AR (2009) Characteristics of rain integral parameters during tropical convective, transition, and stratiform rain at Gadanki and its application in rain retrieval. J Appl Meteor Climatol 48:1245–1266. https://doi.org/10.1175/2008JAMC1948.1
Tang Q, Xiao H, Guo C, Feng L (2014) Characteristics of the raindrop size distributions and their retrieved polarimetric radar parameters in northern and southern China. Atmos Res 135–136:59–75. https://doi.org/10.1016/j.atmosres.2013.08.003
Tao WK, Lang S, Zemg X, Shige S, Takayabu Y (2010) Relating convective and stratiform rain to latent heating. J Clim 23(7):1874–1893
Tapiador FJ, Checa R, de Castro M (2010) An experiment to measure the spatial variability of rain drop size distribution using sixteen laser disdrometers. Geophys Res Lett. https://doi.org/10.1029/2010GL044120
Teschl F, Randeu WL, Schönhuber M, Teschl R (2008) Simulation of polarimetric variables in rain at S-, C- and X-band wavelengths. Adv Geosci 16:27–32. https://doi.org/10.5194/adgeo-16-27-2008
Thompson EJ, Rutledge SA, Dolan B, Thurai M (2015) Drop size distributions and radar observations of convective and stratiform rain over the equatorial Indian and West Pacific oceans. J Atmos Sci 72:4091–4125. https://doi.org/10.1175/JAS-D-14-0206.1
Thompson EJ, Rutledge SA, Dolan B, Thurai M, Chandrasekar V (2018) Dual-polarization radar rainfall estimation over tropical oceans. J Appl Meteorol Climatol 57:755–775. https://doi.org/10.1175/JAMC-D-17-0160.1
Thurai M, Gatlin PN, Bringi VN (2016) Separating stratiform and convective rain types based on the drop size distribution characteristics using 2D video disdrometer data. Atmos Res 169:416–423. https://doi.org/10.1016/j.atmosres.2015.04.011
Tokay A, Short DA (1996) Evidence from tropical raindrop spectra of the origin of rain from stratiform versus convective clouds. J Appl Meteorol 35:355–371. https://doi.org/10.1175/1520-0450(1996)035%3c0355:EFTRSO%3e2.0.co;2
Tokay A, Short DA, Williams CR, Ecklund WL, Gage KS (1999) Tropical rainfall associated with convective and stratiform clouds: intercomparison of disdrometer and profiler measurements. J Appl Meteorol Climatol 38:302–320. https://doi.org/10.1175/1520-0450(1999)038%3c0302:TRAWCA%3e2.0.CO;2
Tokay A, Petersen WA, Gatlin P, Wingo M (2013) Comparison of raindrop size distribution measurements by collocated disdrometers. J Atmos Ocean Technol 30:1672–1690. https://doi.org/10.1175/JTECH-D-12-00163.1
Tokay A, Wolff DB, Petersen WA (2014) Evaluation of the new version of the laser-optical disdrometer OTT Parsivel. J Atmos Ocean Technol 31:1276–1288. https://doi.org/10.1175/JTECH-D-13-00174.1
Ulbrich CW (1983) Natural variations in the analytical form of the raindrop size distribution. J Clim Appl Meteorol 22:1764–1775. https://doi.org/10.1175/1520-0450(1983)022%3c1764:NVITAF%3e2.0.co;2
Ulbrich CW, Atlas D (2007) Microphysics of raindrop size spectra: tropical continental and maritime storms. J Appl Meteorol Climatol 46:1777–1791. https://doi.org/10.1175/2007JAMC1649.1
Ulbrich CW, Lee LG (1999) Rainfall measurement error by WSR-88D radars due to variations in Z-R law parameters and the radar constant. J Atmos Ocean Technol 16:1017–1024. https://doi.org/10.1175/1520-0426(1999)016%3c1017:RMEBWR%3e2.0.co;2
Villarini G, Serinaldi F, Krajewski WF (2008) Modeling radar-rainfall estimation uncertainties using parametric and non-parametric approaches. Adv Wat Res 31(12):1674–1686. https://doi.org/10.1016/j.advwatres.2008.08.022

Vivekanandan J, Adams WM, Bringi VN (1991) Rigorous approach to polarimetric radar modelling of hhydrometeor orientation distributions. J Appl Meteorol and Clim 30:1053–1063. https://doi.org/10.1175/1520-0450(1991)030%3c1053.RATPRM%3e2.0.co;2

Voormansik T, Cremonini R, Post P, Mosseev D (2020) Use of dual-polarization weather radar quantitative precipitation estimation for climatology. Hydrol Earh Syst Sci Discuss. https://doi.org/10.5194/hess-2019-624

Waterman PC (1971) Symmetry, unitarity, and geometry in electromagnetic scattering. Phys Rev D 3:825–839. https://doi.org/10.1103/PhysRevD.3.825

Wu W, Zou H, Shan J, Wu S (2018) A dynamical Z-R relationship for precipitation estimation based on radar echo-top height classification. Adv Meteorol 2018:1–11. https://doi.org/10.1155/2018/8202031

You C-H, Kang M-Y, Hwang Y, Yee J-J, Jang M, Lee D-I (2018) A statistical approach to radar rainfall estimates using polarimetric variables. Atmos Res 209:65–75. https://doi.org/10.1016/jatmosres.2018.03.016

You C-H, Suh S-H, Jung W, Kim H-J, Lee D-I (2022) Dual-polarization radar-based quantitative precipitation estimation of mountain terrain using multi-disdrometer data. Remote Sens 14(10):22190. https://doi.org/10.3390/rs14102290

Yuter SE, Houze RA Jr (1997) Measurement of raindrop size distribution over the Pacific warm pool and implications for Z-R relations. J Appl Meteorol Clim 36:847–867. https://doi.org/10.1175/1520-0450(1997)036%3c0847:MORSDO%3e2.0.co;2

Zeng Q, Zhang Y, Lei H, Xie Y, Gao T, Zhang L, Wang C, Huang Y (2019) Microphysical characteristics of precipitation during pre-monsoon, monsoon, and post-monsoon periods over the South China Sea. Adv Atmos Sci 36:1103–1120. https://doi.org/10.1007/s00376-019-8225-8

Zhang Y, Liu L, Bi S, Wu Z, Shen P, Ao Z, Chen C, Zhang Y (2019) Analysis of dual-polarimetric radar variables and quantitative precipitation estimators for landfall typhoons and squall lines based on disdrometer data in Southern China. Atmosphere 10:30. https://doi.org/10.3390/atmos10010030

Zrnić DS, Keenan TD, Carey LD, May P (2000) Sensitivity analysis of polarimetric variables at a 5-cm wavelength in rain. J Appl Meteor Climatol 39:1514–1526. https://doi.org/10.1175/1520-0450(2000)039%3c1514:SAOPVA%3e2.0.CO;2

Publisher's Note